Theoretical transition probabilities for the $\tilde{A}\,^1\Pi$-$\tilde{X}\,^1\Sigma^+$ system of AlNC and AlCN isomers based on global potential energy surfaces

Ikuo Tokue[a)]
Department of Chemistry, Faculty of Science, Niigata University, 2-8050 Ikarashi, Niigata 950-2181, Japan

Shinkoh Nanbu
Computing and Communications Center, Kyushu University, 6-10-1 Hakozaki, Fukuoka 812-8581, Japan

(Received 14 March 2006; accepted 1 May 2006; published online 8 June 2006)

Transition probabilities were evaluated for the $\tilde{X}\,^1\Sigma^+$-$\tilde{A}\,^1\Pi$ system of AlNC and AlCN isomers to analyze photoabsorption and fluorescence spectra. The global potential energy surfaces (PESs) of the $\tilde{X}\,^1\Sigma^+$ and $\tilde{A}\,^1\Pi$ ($1\,^1A'',2\,^1A'$) electronic states were determined by the multireference configuration interaction calculations with the Davidson correction. Einstein's B coefficients were computed by quantum vibrational calculations using the three-dimensional PESs of these states and the electronic transition moments for the $\tilde{X}$-$1\,^1A''$ and $\tilde{X}$-$2\,^1A'$ systems. Einstein's B coefficients obtained for AlNC or AlCN exhibit that the Al–N or Al–C stretching mode is strongly enhanced in the transition. The absorption and fluorescence spectra calculated for the $\tilde{X}$-$1\,^1A''$ and $\tilde{X}$-$2\,^1A'$ systems are discussed comparing with the observed photoexcitation and fluorescence spectra. The lifetimes for the several vibrational levels of the $\tilde{A}\,^1\Pi$ state were calculated to be ca. 7 ns for AlNC and 21–24 ns for AlCN from the fluorescence decay rates of the $1\,^1A''$-$\tilde{X}$ and $2\,^1A'$-$\tilde{X}$ emissions.
 [DOI: 10.1063/1.2207611]

I. INTRODUCTION

In recent years, much attention has been directed to metal cyanide/isocyanide molecules (MCN/NC) through spectroscopic and theoretical studies from astronomical and reaction mechanismic points of view. The structures and reactions of the alkali molecules have been explained from the nearly isotropic nature of the interaction of a metal ion with the cyanide anion.[1–4] The experimental and theoretical studies of the corresponding alkaline earth molecules (M=Mg, Ca, Sr) showed that all these species have a linear structure including the first excited state.[5–14] The ground and first excited states are still characterized by ionic bonding and the potential energy curves along the bending coordinate are relatively isotropic. Moreover, large amplitude motions (LAMs) often appear in excited rovibrational levels of MCN/MNC. The LAM plays an important role of the unimolecular reaction in the gas phase and the intermolecular vibrational redistribution process.[13,15] Nanbu *et al.*[13] studied the theoretical absorption and emission spectra of the $\tilde{X}\,^2\Sigma^+$-$\tilde{A}\,^2\Pi$ system for CaNC/CN by performing time-dependent quantum mechanical calculations on the potential energy surfaces (PESs) of the related states. They pointed out that the characteristics of the observed spectra by Scurlock *et al.*[12] originated in the Renner-Teller (RT) splitting.

It is also interesting to consider cyanides involving trivalent metals because of increasing the covalent character. Ma *et al.*[16] have employed quantum mechanical methods to study the ground electronic state of the AlNC and AlCN isomers and the transition state between these two structures. They also calculated vibrational and rotational constants for both isomers. Rotational transitions of AlNC have been reported by Robinson *et al.*[17] and Walker and Gerry.[18] These studies show that the ground state has a linear and fairly rigid AlNC structure. Fukushima[19] observed the laser induced fluorescence (LIF) spectra from AlNC/AlCN generated in supersonic free expansions. He assigned the dispersed fluorescence spectra with the band origin at 28 754 cm^{-1} to the progressions of the AlNC($\tilde{A}\,^1\Pi$-$\tilde{X}\,^1\Sigma^+$) transition and related the congested bands to the isomerization reaction, AlNC↔AlCN. He also determined the vibrational constants of the $\tilde{X}$ state. Later, Gerasimov *et al.*[20] observed the AlNC($\tilde{A}\,^1\Pi$-$\tilde{X}\,^1\Sigma^+$) transition in the 35 800–37 700 cm^{-1} region and determined the vibrational constants of the $\tilde{X}$ state. They also observed the 28 754 cm^{-1} band, assigned to AlNC by Fukushima, and concluded that the molecular carrier of this transition is attributed to the AlCN isomer. Mok *et al.*[21] calculated the geometries and the harmonic vibrational frequencies for these electronic states employing several methods. They simulated the theoretical fluorescence spectra arising from the Al–N stretching modes (ν_3=0,1,2) of the upper state based on the harmonic Franck-Condon factors (FCFs) and assigned the spectra observed by Gerasimov *et al.*[20] to the $\tilde{A}\,^1\Pi$-$\tilde{X}\,^1\Sigma^+$ transition of AlNC. Nevertheless, to our knowledge, it seems that information on the electronic states and their vibrational structures of AlNC/AlCN molecule especially the excited states is still insufficient.

In this paper, we outline *ab initio* molecular orbital configuration interaction (MO CI) calculations used in our de-

a)Author to whom correspondence should be addressed. Fax: +81-25262-6116. Electronic mail: itok-pc@chem.sc.niigata-u.ac.jp

termination of the three-dimensional PESs as well as quantum vibrational calculations. Subsequently, we describe the PESs for the $\tilde{X}\,^1\Sigma^+$ and $\tilde{A}\,^1\Pi$ ($1\,^1A'', 2\,^1A'$) states and also vibrational levels for each electronic state. Next, the FCFs and Einstein's A and B coefficients between these states were calculated. The fluorescence lifetimes for the $1\,^1A''$ and $2\,^1A'$ states were obtained from the inverse of the state sum of fluorescence decay rate. Finally, the theoretical absorption and emission spectra of the $\tilde{X}\,^2\Sigma^+$-$\tilde{A}\,^2\Pi$ system based on the transition probabilities are summarized and discussed comparing with the observed spectra.[19,20] The main purpose of this paper is to elucidate the photoexcitation and fluorescence mechanisms of AlNC and AlCN more precisely.

II. THEORY

A. *Ab initio* MO CI calculations

Determination of the global PES is quite important to calculations of the higher vibrational states, as it is necessary to take into account the anharmonicity of the PES, especially for the electronic excited states. The basis set used in the present work was the diffusion-function-augmented, correlation consistent, polarized valence, triple zeta (aug-cc-pVTZ) of Woon and Dunning.[22] The MOs were determined by complete active space self-consistent-field (CASSCF) calculations. After determining the MOs, multireference configuration interaction (MRCI) calculations were carried out.

AlNC is a 26-electron system, and the ground state for the valence is approximated by the wave function

$$[\text{core}](6\sigma)^2(7\sigma)^2(2\pi)^4(8\sigma)^2(9\sigma)^2 \quad \tilde{X}\,^1\Sigma^+,$$

for both linear AlNC and AlCN, and

$$[\text{core}](7a')^2(8a')^2(9a')^2(2a'')^2(10a')^2(11a')^2 \quad \tilde{X}\,^1A',$$

for the bending conformation.

The first excited singlet state for linear AlNC/CN is an open shell and the corresponding configurations are

$$[\text{core}](6\sigma)^2(7\sigma)^2(8\sigma)^2(2\pi)^4(9\sigma)^1(3\pi)^1 \quad \tilde{A}\,^1\Pi,$$

and

$$[\text{core}](7a')^2(8a')^2(9a')^2(2a'')^2(10a')^2(11a')^1(3a'')^1 \quad 1\,^1A'',$$

$$[\text{core}](7a')^2(8a')^2(9a')^2(2a'')^2(10a')^2(11a')^1(12a')^1 \quad 2\,^1A',$$

for the bending conformation. The $1\,^1A''$ and $2\,^1A'$ states are a RT pair.

To obtain the MOs necessary to describe these electronic states, the state-averaged CASSCF calculations were carried out with inclusion of a full valence as the active space orbitals. The active space of the MRCI calculations is the same as that of CASSCF, and the configuration state functions were generated by single and double excitations with respect to the reference configurations used in the CASSCF calculation, except for the frozen-core orbitals, $1s$, $2s$, and $2p$ (Al). Moreover, the Davidson correction for the MRCI calculation was employed to include the correlation energy due to higher excitations.[23–25] In the present work, the potential energies for the electronic ground state, $1\,^1A'$, and the next two electronic excited states, $1\,^1A''$ and $2\,^1A'$, were finally obtained in the C_s symmetry. The total number of configurations for the final internally contracted MRCI calculations[26,27] was $(4-14)\times10^6$ for the A' symmetry and $(3-13)\times10^6$ for the A'' symmetry. The transition dipole moments between these states were evaluated from the CI wave functions. All of the *ab initio* calculations were performed using the MOLPRO 2002.6 program package.[28] The calculations were mainly carried out on the SX7 and TX7 computers of the Research Center for Computational Science of The Okazaki National Institutes. Each data point required about 12 h of CPU time.

Jacobi coordinates were employed to describe the relative positions of the three nuclei in the body fixed plane; r is the distance between C and N atom, R is the distance between the Al atom and the center of mass of C and N atoms, and θ is the angle between the vectors R and r. Potential energies and transition dipole moments were finally calculated at 1500 geometries and were interpolated by the interpolant moving least squares method combined with the Shepard method[29–31] to carry out a quantum vibrational calculation on the PESs. The parameters to determine the weight functions [see Eq. (6) of Ref. 29] were chosen to be $a=0.03$ and $p=4$.

B. Quantum vibrational calculations

Since some of the highly vibrational excited states could be characterized with the unlocalized wave function that does not look like the zero-point vibrational wave function, we performed a quantum vibrational calculation based on the discrete variable representations.[32–35] The Hamiltonian operator H may be written formally as[36]

$$H=\frac{P_R^2}{2\mu_R}+\frac{p_r^2}{2\mu_r}+\frac{(\mathbf{J}-\mathbf{j})^2}{2\mu_R R^2}+\frac{\mathbf{j}^2}{2\mu_r r^2}+V(R,r,\cos\theta), \quad (1)$$

where $\mu_R=m_{\text{Al}}(m_{\text{C}}+m_{\text{N}})/(m_{\text{Al}}+m_{\text{C}}+m_{\text{N}})$, $\mu_r=m_{\text{C}}m_{\text{N}}/(m_{\text{C}}+m_{\text{N}})$, P_R and p_r are appropriate radial momentum operators associated with R and r, and $\mathbf{J}$ and $\mathbf{j}$ denote the total angular momentum and CN angular momentum operators.

The Hamiltonian matrix and associated wave functions are represented with evenly spaced grids in R and r, and associated Legendre polynominals to describe $\cos\theta$. The grid parameters were suitable for the radial part: ($N_R=139$, $R_{\min}=1.0a_0$, $R_{\max}=8.0a_0$) and ($N_r=79$, $r_{\min}=1.0a_0$, $r_{\max}=5.0a_0$), where N is the number of grid points and a_0 is the Bohr radius. The number of Legendre functions was 70 for the angular part. The method adopted for the diagonalization of the Hamiltonian matrix is the implicitly restricted Lanczos method.[37] In the present work, assuming the total angular momentum $J=0$ and 1, the lowest 350 vibrational states were obtained for the three electronic states of AlNC/CN. The FCFs were then evaluated as the square of the overlap integrals between the initial and final states for the $\tilde{X}$-$1\,^1A''$ and $\tilde{X}$-$2\,^1A'$ systems, and Einstein's B coefficients for photoabsorption[38] were also calculated as the square of the transition moments that depend on both the initial and final vibrational states. Finally, Einstein's A coefficients were evaluated from the transition energies and Einstein's B coefficients.

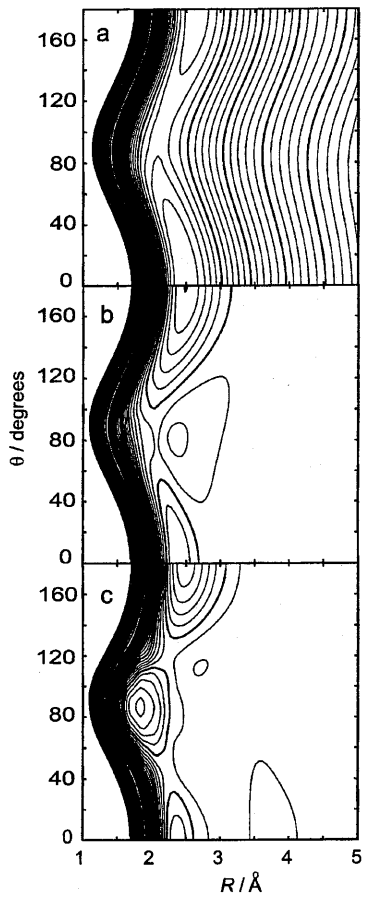

FIG. 1. Potential energy surfaces for the (a) $\tilde{X}\,^1\Sigma^+$, (b) $1\,^1A''$, and (c) $2\,^1A'$ states for AlNC/AlCN; r is fixed at the equilibrium distance of 1.188 Å for the ground state. Narrow and thick contours are shown in the intervals of 0.2 and 1.0 eV, respectively.

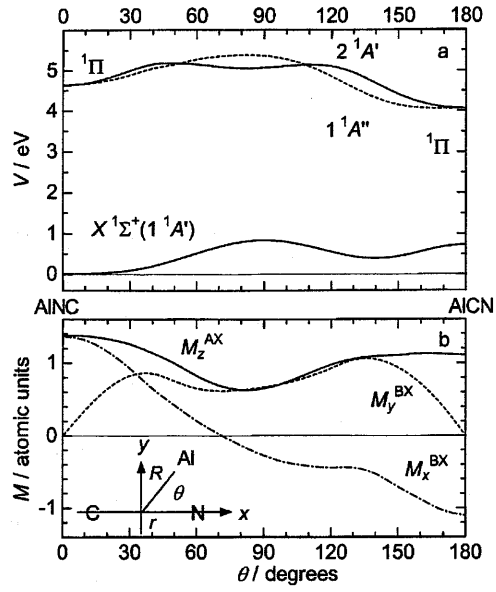

FIG. 2. (a) Potential energies for the $\tilde{X}\,^1\Sigma^+$, $1\,^1A''$, and $2\,^1A'$ states in eV and (b) transition dipole moments, M, as a function of θ.

III. RESULTS AND DISCUSSION

A. Potential energy surfaces

Figure 1 shows the two-dimensional PESs of the $\tilde{X}\,^1A'$, $1\,^1A''$, and $2\,^1A'$ states, where r is fixed at the equilibrium length of 1.188 Å for the ground state. The energy zero of each electronic state is taken to be at the global energy minimum of the corresponding state; $\tilde{X}$, $1\,^1A''$, and $2\,^1A'$ states are −334.693 700, −334.548 638, and −334.551 343 E_h, respectively. Figure 2 shows the potential energy curves of the three lowest states for AlNC and AlCN and the dependence of the transition dipole moments, M, on θ and R. In Fig. 2(a), it is clearly seen that the $1\,^1A''$ and $2\,^1A'$ states are the RT pair derived from the $\tilde{A}\,^1\Pi$ state. The potential function for the $1\,^1A''$ state is the lower one and that for the $2\,^1A'$ state is the higher one around the linear geometry, whereas these states cross each other around $\theta=50°$ and 110° and then the $2\,^1A'$ state has a global minimum around $\theta=90°$; we call this geometry the T-shaped AlNC in this paper.

The equilibrium geometry of each state was evaluated via polynomial fit for the potential energy data. Table I summarizes the geometries thus determined compared with the published data. The geometries of the ground state obtained in this study are in good agreement with recent theoretical data, whereas those of the $\tilde{A}\,^1\Pi$ state are slightly different from the previous values.[16,19,21,39] The global minimum for the $\tilde{X}$ state is the linear AlNC and the energy difference with the linear AlCN is 0.224 eV. The transition state for the isomerization reaction of $\mathrm{AlNC}(\tilde{X}) \leftrightarrow \mathrm{AlCN}(\tilde{X})$ is around $r=1.19$, $R=2.14$ Å, and $\theta=104°$, and its barrier height was estimated to be 0.52 eV from the global minimum of AlNC. The geometrical character of the transition state is in good agreement with the 0.57 eV barrier reported by Ma *et al.*[16] For the $\tilde{A}\,^1\Pi$ state, the linear AlCN is about 0.593 eV more stable than the linear AlNC. Our E_e energy of 4.574 eV calculated for the $\tilde{A}\,^1\Pi$ state of AlNC agrees well with the observed E_0 value of 4.512 eV.[20] The transition state for the PES of the $1\,^1A''$ state is around $r=1.19$, $R=2.07$ Å, and $\theta=78°$, and its barrier height was estimated to be 1.22 eV from the global minimum of $\mathrm{AlCN}(\tilde{A}\,^1\Pi)$. The PES of the $2\,^1A'$ state has two transition states around $\theta=45$ and 122° with the barrier of 1.05 and 1.03 eV, respectively. The excitation energy from the $\tilde{X}$ state to the $\tilde{A}$ state for AlCN is evaluated to be 3.723 eV, which is consistent with 3.77 eV calculated by Chau *et al.*[39] and the observed E_0 of 3.565 eV.[19,20]

To clarify the spin-orbit (SO) interactions, the SO matrix elements and eigenstates were computed using the Breit-Pauli operator within the MRCI program of MOLPRO program package. The basis set used in this calculation was the Stuttgart relativistic large core effective core potential (Ref. 40) for Al atom and the cc-pVDZ (Ref. 41) for C and N atoms. The energies of the $\tilde{X}$ and $\tilde{A}$ states calculated including the SO coupling were almost equal to the MRCI values neglecting the SO coupling around the linear AlNC and AlCN. Moreover, the $\tilde{A}\,^1\Pi$ state does not seem to intersect with any triplet state at lower energy region. Therefore, we concluded that the SO effects are negligible on the $\tilde{X}$ and $\tilde{A}$ states and their vibrational levels around the energy region interested in this study.

TABLE I. Equilibrium geometries and electronic energies of the $\tilde{X}\,^1\Sigma^+$ and $\tilde{A}\,^1\Pi$ ($1\,^1A''$ and $2\,^1A'$) states; bond lengths are in Å, angles are in °, and the energy difference (E_e) form the ground state of AlNC in eV.

Geometry	r	R	θ	$r_{\mathrm{Al-N}}$	$r_{\mathrm{Al-C}}$	E_e	Method
				$\tilde{X}\,^1\Sigma^+$			
AlNC	1.188	2.422	0.0	1.874	3.062		MRCI/aug-cc-pVTZ[a]
	1.187	2.409	0.0	1.861	3.048		CCSD(T)/TZ2p+f[b]
	1.188	2.412	0.0	1.864	3.052		QCISD(T)/6-311+G(3df)[c]
	1.178	2.403	0.0	1.859	3.037		QCISD/cc-pVQZ[d]
AlCN	1.173	2.661	180.0	3.202	2.030	0.224	MRCI/aug-cc-pVTZ[a]
	1.171	2.645	180.0	3.185	2.014	0.239	CCSD(T)/TZ2p+f[b]
	1.171	2.260	180.0	3.193	2.022	0.245	QCISD(T)/6-311+G(3df)[c]
	1.161	2.436	180.0	3.183	2.022		QCISD/cc-pVQZ[e]
				$\tilde{A}\,^1\Pi$			
AlCN	1.186	2.528	180.0	3.076	1.889	3.947	MRCI/aug-cc-pVTZ[a]
	1.158	2.541	180.0	3.075	1.917		QCISD/cc-pVQZ[e]
AlNC	1.207	2.341	0.0	1.748	2.991	4.540	MRCI/aug-cc-pVTZ[a]
	1.175	2.443	0.0	1.859	2.985	4.574	QCISD/cc-pVQZ[d]
						4.512	LIF[f]
T shaped[a]	1.268	1.796	87.9	1.868	1.897	3.874	MRCI/aug-cc-pVTZ[a]
	1.224	1.851	86.2	1.895	2.011	3.643	QCISD/6-311+G(3df)[c]

[a]This work.
[b]Reference 16.
[c]Reference 19.
[d]Reference 21.
[e]Reference 39.
[f]E_0 value from Ref. 20.

In Fig. 2(b), the M_z^{AX} is the transition dipole moment for the $1\,^1A''$-$\tilde{X}$ system, and the M_x^{BX} and M_y^{BX} are those for the $2\,^1A'$-$\tilde{X}$ systems. Figure 3 shows the two-dimensional surfaces of the absolute transition moments. The M_y^{BX} becomes zero at the linear geometry and M_x^{BX} changes the sign around θ=72°. Both M_z^{AX} and M_x^{BX} with r=1.2 Å have a maximum around R=2.4 Å for AlNC and R=2.6 Å for AlCN and rapidly decrease when R deviates from the equilibrium length. These features indicate that the bands to higher vibrational levels in the Al–N or Al–C stretching mode are more suppressed than the FC envelopes in the $\tilde{X}$-$1\,^1A''$ and $\tilde{X}$-$2\,^1A'$ photoexcitations.

B. Vibrational analysis

Vibrational energies were calculated up to 350 levels with J=0 and 1 for the three electronic states; the vibrational energies for the 350th level with J=0 of the $\tilde{X}$, $1\,^1A''$, and $2\,^1A'$ states are 7060, 9020, and 8660 cm^{-1}, respectively, from each potential minimum. For all the electronic states of the linear AlNC, linear AlCN, and T-shaped AlNC, the vibrational levels have been assigned as the vibrational quantum numbers (ν_1,ν_2,ν_3); the r stretching ν_1, bending ν_2, and R stretching ν_3 modes. All vibrational wave functions were successfully assigned except the strongly mixed wave functions, which correspond to LAM and entirely spread to the bending coordinate. To certify the assignment, a least-square analysis was applied to the vibrational frequencies using the well-known formula for three normal vibrations including anharmonicity constants; the vibrational frequency in reference to the vibrational ground state is given by[42]

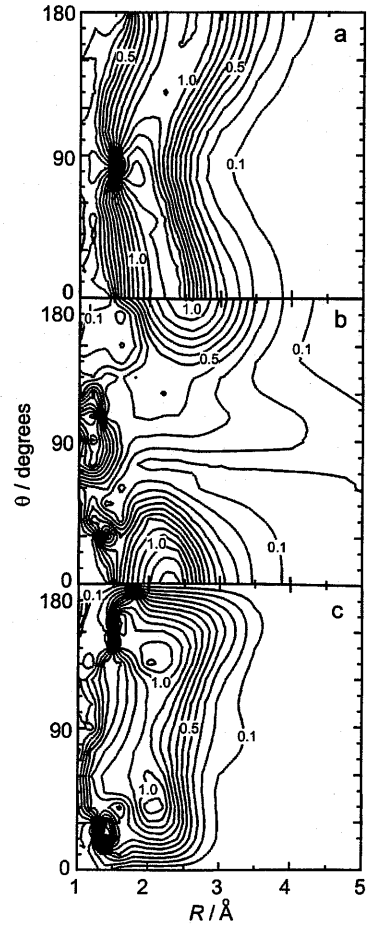

FIG. 3. Absolute transition moment surfaces for (a) M_z^{AX}, (b) M_x^{BX}, and (c) M_y^{BX}; r is fixed 1.2 Å.

TABLE II. Vibrational (G) and vibronic (T) energies of the $\tilde{X}\,^1\Sigma^+$, $1\,^1A''$, and $2\,^1A'$ states for the linear AlNC in cm^{-1}; C–N str. ν_1, bend ν_2, and Al–N str. ν_3.

	$\tilde{X}\,^1\Sigma^+$		$1\,^1A''$			$2\,^1A'$			
	Calc.[a]	Obs.[b]	Calc.[a]		Obs.[b]	Calc.[a]		Obs.[c]	
(ν_1,ν_2,ν_3)	G	G	T^c	G	G	T^c	G	G	
(0,0,0)	0	0	4912	0	0	5627	0	0,	0
(0,1,0)	118		5097	180		5899	271	371,	288
(0,2,0)	229	200	5268	351	284	6150	523	659,	606
(0,3,0)	342		5441	523		6408	780	977,	⋯
(0,4,0)	450	400	5606	689	592	6652	1025		
(0,5,0)	560		5773	856		6898	1271		
(0,6,0)	665	600	5934	1017					
(0,0,1)	541	549	5496	604	598	6186	559	⋯,	596
(0,1,1)	667		5682	765		6461	834		
(0,2,1)	785	760	5859	941	890	6719	1092		
(0,3,1)	904		6036	1119		6978	1351		
(0,4,1)	1016	971	6204	1287	1197				
(0,0,2)	1070	1098	6094	1177	1174	6774	1146		
(0,1,2)	1204		6284	1367		7050	1432		
(0,2,2)	1328	1320	6465	1548					
(0,3,2)	1453		6645	1728					
(0,0,3)	1592	1647	6677	1759					
(0,0,4)	2105	2196	7220	2303					
(0,0,5)	2621	2745							
(0,0,6)	3127	3294							
(1,0,0)	2042	2069	6724	1806					
(1,0,1)	2582	2618	7296	2379					
(1,0,2)	3110	3167							

[a]Levels with ν_2=even and odd corresponds to the state with J=0 and 1, respectively, in this study; T means the energy from the vibrational ground level of each electronic state.
[b]Reference 20.
[c]First value from Ref. 20 and second is the value reassigned in this study.

$$G(\nu_1,\nu_2,\nu_3)=\sum_{i=1}^{3}\omega_i^0\nu_i+\sum_{i=1}^{3}\sum_{k\geqslant i}^{3}x_{ik}^0\nu_i\nu_k. \quad (2)$$

For the linear AlNC and AlCN, the linear notation of bending vibrational quantum state was applied for the bending modes (ν_2). The pure stretching levels were well fitted by the formula, whereas the combination levels with $\nu_1+\nu_3\geqslant 6$ were found to be deviated from Eq. (2) indicating strong couplings among these stretching modes. Moreover, the $\nu_2\geqslant 14$ levels were deviated definitely from this formula. Therefore, we added the third order anharmonicity constants y_{222} to Eq. (2). We should take Coriolis coupling into account for the rigorous analysis since the vibrational energies calculated for the levels with J=1 include the Coriolis interaction. Nevertheless, we neglected the effect of Coriolis interaction in the vibrational analysis because our goal of this study is to describe the feature of the $\tilde{X}$-$1\,^1A''$ and $\tilde{X}$-$2\,^1A'$ transitions as a whole.

To examine the accuracy of the PESs, especially concerning the ν_3 mode, the vibrational frequencies obtained in this study are compared with the observed data.[19,20] Table II summarizes the vibrational energies of the three states with J=0 and 1 for AlNC and Table III summarizes those for AlCN. For the $\tilde{X}$ state, the vibrational energies of bending modes calculated for both AlNC and AlCN are about 10% higher than the observed. Moreover, those for the pure ν_3 mode are lower than the observed; the difference between the calculated and observed energies of the (0,0,6) level reaches to 5% for AlNC and to 10% for AlCN. Nevertheless, the present results of the $\tilde{X}$ state agree entirely with the observed values for both AlNC and AlCN. Gerasimov *et al.*[20] concluded that the vibrational energies determined by Fukushima corresponds to AlCN. The present results for the $\tilde{X}$ state of AlNC are roughly intermediate those observed by Fukushima[19] and Gerasimov *et al.*[20] Therefore we cannot decide the emitter observed by Fukushima is either AlCN or not unless we consider the electronic transition energy.

The vibrational energies calculated for the $1\,^1A''$ and $2\,^1A'$ states agree well with the observed values by Gerasimov *et al.*[20] except those for bending levels. Taking into account of the transition energy T_0 and the profile of the emission spectra, we reassigned all the spectra, which were attributed to the $\tilde{X}$-$2\,^1A'$ transition by Gerasimov *et al.* The detail of the reassignment will be described in the next section. The agreement of the calculated energies for the bending levels of the $2\,^1A'$ state with the observed was improved by the reassignment; the vibrational energies evaluated by the reassignment were shown in the second row. Hereafter, we write the bending levels of the $1\,^1A''$ and $2\,^1A'$ state as ν_2^- and ν_2^+, respectively, for convenience.

TABLE III. Vibrational (G) and vibronic (T) energies of the $\tilde{X}\,^1\Sigma^+$, $1\,^1A''$, and $2\,^1A'$ states for the linear AlNC in cm^{-1}; C–N str. ν_1, bend ν_2, and Al–N str. ν_3.

	$\tilde{X}\,^1\Sigma^+$			$1\,^1A''$	$2\,^1A'$	
	Calc.[a]		Obs.[b]	Calc.[a]	Calc.[a]	
(ν_1,ν_2,ν_3)	T	G	G	$T(=G)$	T	G
(0,0,0)	1842	0	0	0	662	0
(0,1,0)	1990	147		218	988	326
(0,2,0)	2128	285	255, 257	426	1311	649
(0,3,0)	2266	424		636	1633	971
(0,4,0)	2397	554	492, 498	837	1952	1290
(0,5,0)	2528	686		1041	2271	1609
(0,6,0)	2652	810	712, 722	1238	2587	1925
(0,0,1)	2311	467	521, 521	556	1195	533
(0,1,1)	2465	622		778	1516	854
(0,2,1)	2606	764	789, 792	990	1836	1174
(0,3,1)	2747	905		1203	2155	1493
(0,4,1)	2875	1003[c]	1016, 1045	1408	2471	1810
(0,0,2)	2772	929	1039, 1038	1113	1742	1080
(0,1,2)	2930	1088		1340	2058	1396
(0,2,2)	3076	1234	1320, 1322	1554	2372	1710
(0,3,2)	3217	1274		1770	2685	2023
(0,0,3)	3228	1386	1552, 1551	1663	2285	1615
(0,0,4)	3682	1839	2060, 2059	2203	2814	2153
(0,0,5)	4133	2290	2565, 2563	2731	3328	2666
(0,0,6)	4582	2738	3065, 3062	3249	3825	3163
(1,0,0)	3936	2084	1975, 1975	1919	2584	1922
(1,0,1)	4405	2552	2496, 2496	2477	3120	2458
(1,0,2)	4863	3020	3014, 3014	3036	3669	3007

[a]States with ν_2=even corresponds to $J=0$ and those with ν_2=odd to $J=1$.
[b]First value calculated from the vibrational constants in Ref. 19 and second value calculated from those in Ref. 20.
[c]Mixed with the (080) level.

The $1\,^1A''$ and $2\,^1A'$ states are subjected to the RT interaction. The Renner parameter, ε, is a dimensionless constant to describe the RT coupling of the bending potential.[43] The ε parameter may be expressed using the bending frequencies for the two states as[44]

$$\varepsilon = \frac{(\omega_0^+)^2 - (\omega_2^-)^2}{(\omega_2^+)^2 + (\omega_2^-)^2}, \tag{3}$$

where ω^+ and ω^- are the frequencies for the higher and lower states, respectively. The ε value of the $\tilde{A}\,^1\Pi$ state for AlNC estimated from the frequencies calculated for the $(0,\nu_2=1-3,0)$ levels is 0.38 ± 0.02, against 0.63 obtained by the data reassigned in this study. In the same way, the ε parameter for AlCN is calculated to be 0.39 ± 0.02. Thus, it may be concluded that the splitting of the RT pair for AlNC is the same order as that for AlCN.

The discrepancy between the present and observed ε values for AlNC should be caused by the RT coupling because the observed frequencies should correspond to the levels with $J\geqslant 1$. When $J=0$, the RT coupling between the bending levels of the $1\,^1A''$ and $2\,^1A'$ states is rigorously neglected, whereas the RT interaction should be included in the levels with $J>0$ in the rigorous treatment of the vibrational energy and the transition probability. In preliminary calculation with the same method reported by Goldfield and Gray,[34] the RT effect on the vibronic energies was estimated for the states with $J=1$ of AlCN. Table IV lists the results for the states with $J=1$ and $K=1$ including the RT coupling compared with those neglecting the RT effect. Although the RT coupling is found to be not so large for the states with $\nu_2\leqslant 5$, the ε parameter is improved to be 0.57 from the (0,1,0) energies calculated including the RT effect. Of course, it should be needed to calculate the vibrational energies until much higher states both to make sure such an explanation and to calculate the transition probabilities more accurately than this convenient approximation for the RT effect. Unfortunately, the $(0,1^+,0)$ level for AlNC is estimated to be higher than the 300th level in the calculation and then the calculation including much higher levels may exceed our available

TABLE IV. Vibrational energies in cm^{-1} of the states with $J=1$ and $K=1$ for the linear AlCN.

	$1\,^1A''$		$2\,^1A'$	
(ν_1,ν_2,ν_3)	No RT[a]	RT[b]	No RT[a]	RT[b]
(0,1,0)	218	171	326	327
(0,3,0)	636	522	971	973
(0,5,0)	1041	974	1609	1611

[a]Calculation neglecting the RT effect.
[b]Calculation including the RT effect.

TABLE V. Vibrational energies G (=T) in cm^{-1} calculated for the nonrotating 2 $^1A'$ state of the T-shaped AlNC; r str. ν_1, bend ν_2, and R str. ν_3.

(ν_1,ν_2,ν_3)	G	(ν_1,ν_2,ν_3)	G
(0,0,0)	0	(0,0,2)	1352
(0,1,0)	571	(0,1,2)	1884
(0,2,0)	1136	(0,2,2)	2408
(0,3,0)	1695	(0,3,2)	2928
(0,4,0)	2247	(0,0,3)	1980
(0,5,0)	2785	(0,0,4)	2589
(0,6,0)	3308	(0,0,5)	3183
(0,0,1)	700	(0,0,6)	3825
(0,1,1)	1252	(1,0,0)	1509
(0,2,1)	1787	(1,0,1)	2205
(0,3,1)	2314	(1,0,2)	2860
(0,4,1)	2843	(2,0,0)	2978

computational resource. Nevertheless, the energy shifts by the RT effect for AlNC are expected to be similar to those for AlCN based on the Renner parameters for both the geometries. Therefore, we neglected the RT effect in the calculation for the $J=1$ state since the levels with ν_2=odd seem to be not so important in the emission spectra compared with the levels with ν_2=even.

Table V summarizes the vibrational energies with $J=0$ of the 2 $^1A'$ state for the T-shaped AlNC; we cannot find any observed value. Fukushima[19] reported the harmonic frequencies of 1667 cm^{-1} for ω_1, 421 cm^{-1} for ω_2, and 550 cm^{-1} for ω_3 calculated by the QCISD/6-311+G(3df) level. The vibrational frequencies for the first excited levels calculated in this study are fairly different from the harmonic frequencies.

C. Franck-Condon factors and transition probabilities for the $\tilde{X}$-$\tilde{A}$ system

To evaluate the vibrational distribution of the A $^1\Pi$ state in the photoexcitation from the ground and several excited vibrational levels for AlNC and AlCN, the FCFs were calculated for the band from the m state with $(\nu_1'',\nu_2'',\nu_3'')$ to the n state with (ν_1',ν_2',ν_3') of the $\tilde{X}\rightarrow\tilde{A}$ excitation. Moreover, the Einstein's B_{nm} coefficients for the same transition were calculated based on the three-dimensional transition dipole moment. In this study, Einstein's B coefficients for the $m\rightarrow n$ excitation in $m^3\,J^{-1}\,s^{-2}$ units are given by

$$B_{nm}=1.216\,67\times10^{20}|M_{nm}|^2, \tag{4}$$

where the transition moment M_{nm} is in a.u. Einstein's A_{nm} coefficients for the $n\rightarrow m$ band of the $\tilde{A}\rightarrow\tilde{X}$ emission, which are proportional to the cube power of the transition energy, were calculated from Einstein's B coefficients and the differences of the vibronic energies between the two states. The transition dipole moment depends on the molecular geometry as described in Sec. III A, and then the transition probability varies with the vibrational band.

The 1 $^1A''$ and 2 $^1A'$ states are the RT pair as described at the previous section. The lower 1 $^1A''$ and higher 2 $^1A'$ states cross each other at bending geometry and then the 2 $^1A'$ state has a global minimum at θ=88°. Thus, the rovibrational mixing of the 1 $^1A''$ and 2 $^1A'$ states can occur due to the RT coupling, which is a nonadiabatic process. However, in the present work, keeping the adiabaticity of the electronic states, we applied the FC analysis to this system for understanding both the photoexcitation and the photoemission mechanism.

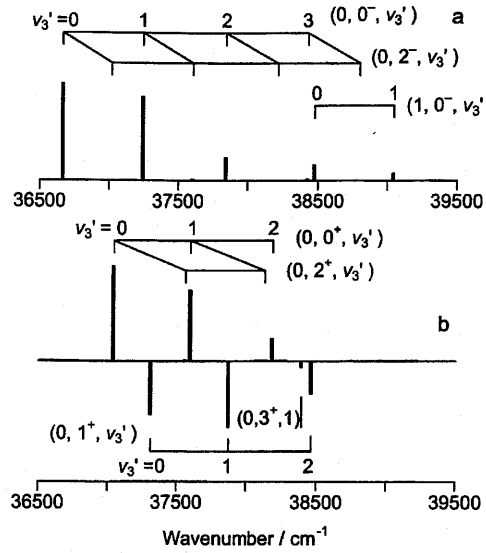

FIG. 4. Theoretical absorption spectra of the (a) $\tilde{X}$-1 $^1A''$ and (b) $\tilde{X}$-2 $^1A'$ systems from the (0,0,0) level for AlNC.

Figure 4 shows the theoretical absorption spectra of the $\tilde{X}$-1 $^1A''$ and $\tilde{X}$-2 $^1A'$ excitations from the (0,0,0) level for AlNC. In the transition the change in r in equilibrium is only 0.02 Å, while that in R is 0.11 Å. Therefore, the main band is the pure ν_3' progression. The bands to the $(0,2,\nu_3')$ and $(1,0,\nu_3')$ levels are next important; these sequences become important in the excitations from higher vibrational levels. The profile for each band almost agrees with the FC envelope for these spectral regions. This means that the transition probability is nearly independent of the vibrational bands as discussed later in detail. The transition energies, T_0, of the $\tilde{X}$-1 $^1A''$ and $\tilde{X}$-2 $^1A'$ systems for AlNC are evaluated to be 36 668 and 37 041 cm^{-1}, respectively, from the zero-point energies of these states. Gerasimov *et al.* assigned the peak at 36 389 cm^{-1} as the band origin of the $\tilde{A}$-$\tilde{X}$ transition.[20] However, the vibrational ground level for the 2 $^1A'$ state should be higher than that for the 1 $^1A''$ state. Therefore, we assigned that the 36 389 cm^{-1} peak as the (0,0,0)-(0,0⁻,0) band. The difference of the T_0 value calculated for the $\tilde{X}$ -1 $^1A''$ transition with the observed is only 280 cm^{-1}. Figure 5 shows the theoretical fluorescence spectra of the AlNC(1 $^1A''$-$\tilde{X}$) emission compared with the observed spectra[20] and Fig. 6 shows those of the AlNC(2 $^1A'$-$\tilde{X}$) emission. The main band is also the pure ν_3'' progression. The bands to the $(1,0,\nu_3'')$ and $(1,2,\nu_3'')$ levels are next important especially in the spectra from higher vibrational levels. The theoretical spectra for the 1 $^1A''$-$\tilde{X}$ emission agree well with the observed spectra except those from the vibrational levels with ν_2=4. The emission spectra from the $(0,0^-,\nu_3'$=0–2) emitters are very similar to those calculated from the harmonic FCFs.[21]

Gerasimov *et al.*[20] assigned the 36 760 cm^{-1} peak as the

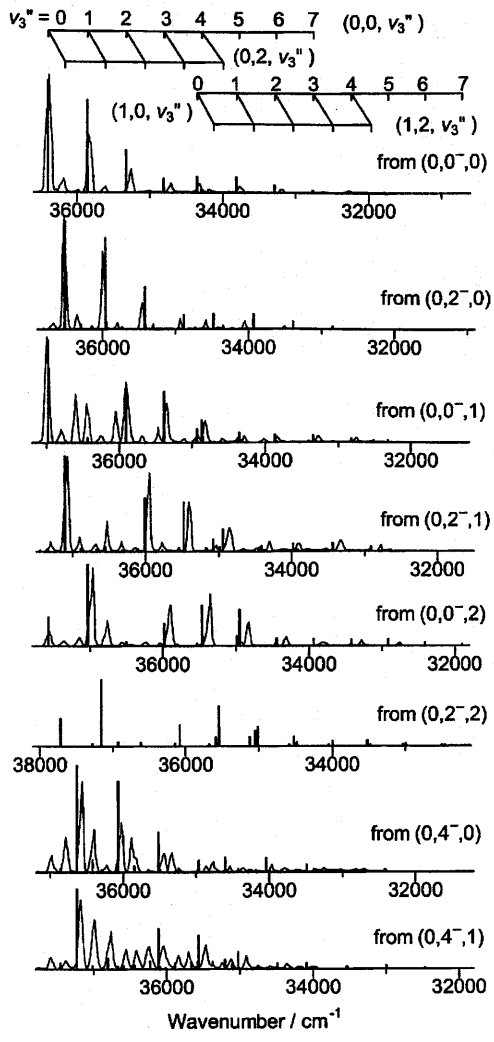

FIG. 5. Theoretical and observed fluorescence spectra of the 1 $^1A''$-$\tilde{X}$ system for AlNC. The wave number for the theoretical spectra are shifted −279 cm^{-1}.

vibronically induced (0,0,0)-(0,1$^+$,0) band, which is 371 cm^{-1} higher than the band origin of the $\tilde{X}$-1 $^1A''$ system. Although the fluorescence spectrum of the 36 760 cm^{-1} band was not shown, we reassigned this band as the (0,0,0) -(0,0$^+$,0) band based on the energy difference between RT pairs for AlNC. Furthermore, Gerasimov *et al.* assigned the 37 048 and 37 366 cm^{-1} peaks in the absorption spectrum as the (0,0,0)-(0,2$^+$,0) and (0,0,0)-(0,3$^+$,0) bands, respectively. However, the FCF for the (0,0,0)-(0,3$^+$,0) band is found to be small. Therefore, the 37 048 and 37 366 cm^{-1} peaks should be reassigned as the (0,0,0)-(0,1$^+$,0) and (0,0,0)-(0,2$^+$,0) bands, respectively, based on the vibrational energies and theoretical fluorescence spectra for the ν_2^+=1 and 2 levels. The theoretical spectrum from the (0,1$^+$,0) level agrees reasonably with the observed 37 048 cm^{-1} emission spectrum adopted from Ref. 20, as shown in Fig. 6. Finally, either the (0,0$^+$,1) or (0,3$^+$,0) level is a candidate for the emitter of the unknown 37 656 cm^{-1} band reported by Gerasimov *et al.* We attributed the (0,0$^+$,1) level to the emitter based on the FCFs for the excitation and the profiles of the emission spectra.

The transition energies, T_0, of the $\tilde{X}$-1 $^1A''$ and $\tilde{X}$-2 $^1A'$

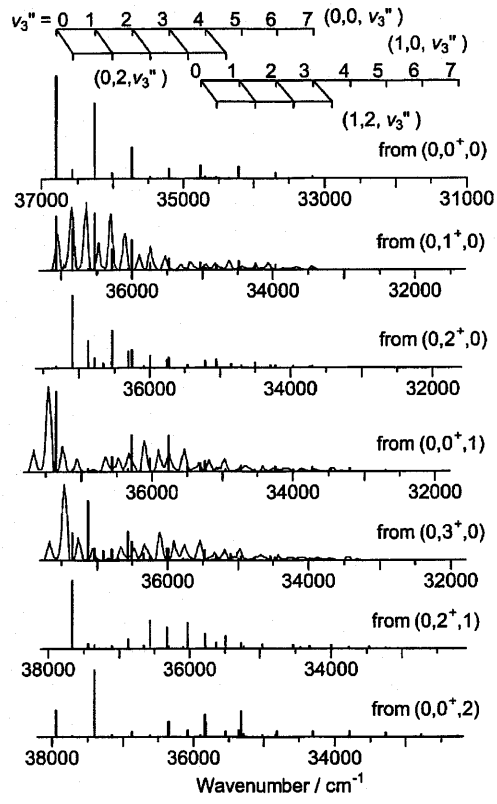

FIG. 6. Theoretical and observed fluorescence spectra of the 2 $^1A'$-$\tilde{X}$ system for AlNC. The wave number for the theoretical spectra are shifted −281 cm^{-1}.

systems for AlCN are evaluated to be 30 036 and 30 233 cm^{-1}, respectively. The T_0 calculated for the $\tilde{X}$ -1 $^1A''$ transition is ca. 1280 cm^{-1} higher than the observed value of 28 754 cm^{-1}. The relatively large discrepancy for AlCN may be caused by the interaction of the $\tilde{A}$ $^1\Pi$ state with the a $^3\Pi$ state. Nevertheless, we found that the energy shift by SO effects is negligible around the linear AlCN, as described in Sec. III A. Figure 7 shows the theoretical absorption spectra of the $\tilde{X}$-1 $^1A''$ and $\tilde{X}$-2 $^1A'$ excitations from the (0,0,0) level for AlCN. In the transition the change in r in

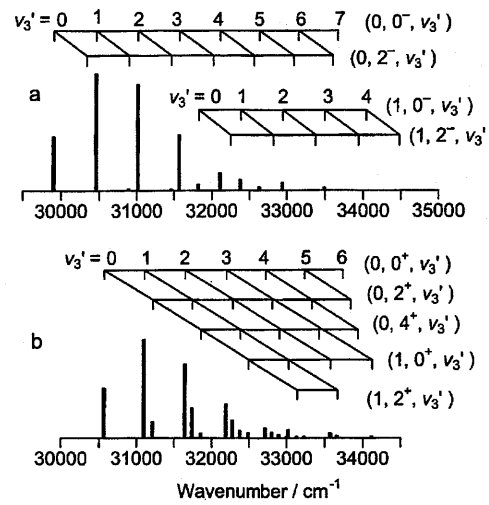

FIG. 7. Theoretical absorption spectra of the (a) $\tilde{X}$-1 $^1A''$ and (b) $\tilde{X}$-2 $^1A'$ systems from the (0,0,0) level for AlCN.

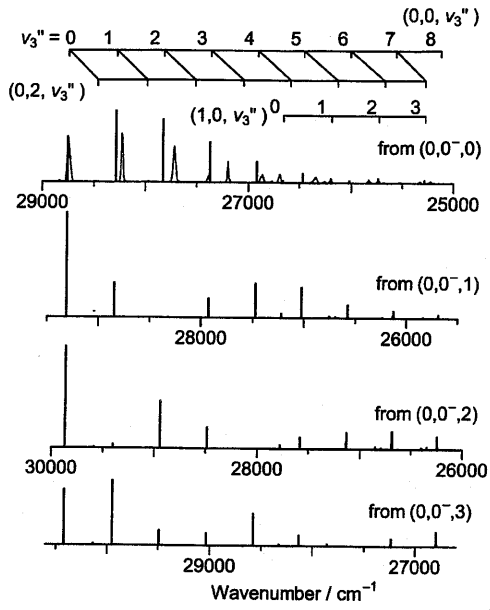

FIG. 8. Theoretical and observed fluorescence spectra of the 1 $^1A''$-$\tilde{X}$ system for AlCN. The wave number for the theoretical spectra are shifted -1280 cm^{-1}.

equilibrium is only 0.01 Å, while that in R is 0.13 Å. Therefore, the main band is the ν_3' progression. The next intense transitions are the bands to the (0, ν_2'=2 and 4, ν_3') and (1, ν_2'=0 and 2, ν_3') levels. Figure 8 shows the theoretical fluorescence spectra of the 1 $^1A''$-$\tilde{X}$ transition for AlCN and Fig. 9 shows those of the 2 $^1A'$-$\tilde{X}$ transition compared with the observed spectra.[19] The main band is also the ν_3'' progression. The vibrational ground levels of the 1 $^1A''$ and $^1A'$ states are candidates for the emitter of the 28 753 cm^{-1} band, which were observed by Fukushima.[19] In the same way, the emitter for the 29 698 cm^{-1} band[19] is attributed as the $(0,0^+,1)$ based on the FC envelope. The energy difference between the band origins for both spectra is reported to be 946 cm^{-1}.

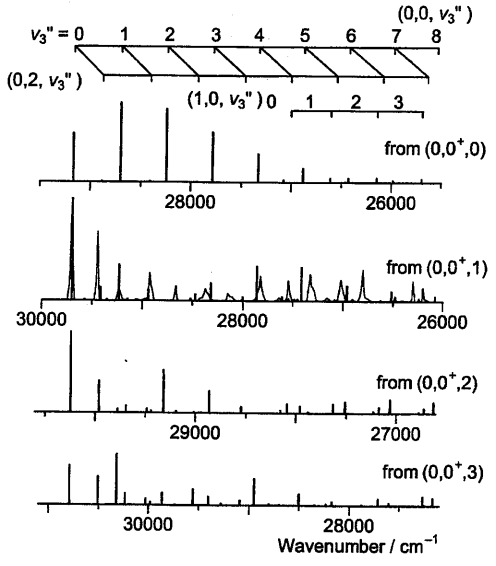

FIG. 9. Theoretical and observed fluorescence spectra of the 2 $^1A'$-$\tilde{X}$ system for AlCN. The wave number for the theoretical spectra are shifted -1068 cm^{-1}.

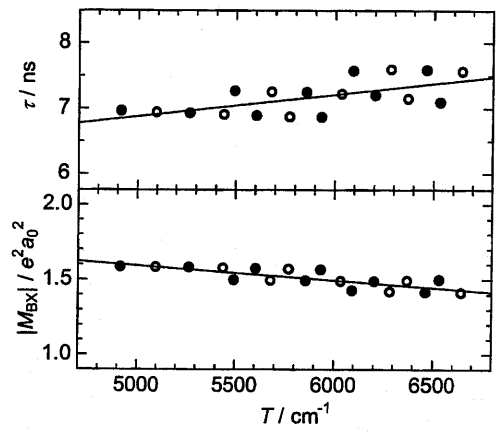

FIG. 10. Dependences of the transition probability for the 1 $^1A''$-$\tilde{X}$ system and the fluorescence lifetime on the vibronic energy T of the 1 $^1A''$ state for AlNC; the filled and open circles represent the vibrational levels with J=0 and 1, respectively.

When the $(0,0^-,0)$ level is the emitter for the 28 753 cm^{-1} band, the energy difference is estimated to be 710 cm^{-1}, which may be within limits allowed. On the other hand, we could not find the emitter for the 29 698 cm^{-1} if the $(0,0^+,0)$ level is attributed to the emitter for the 28 753 cm^{-1} band. Therefore, we prefer the $(0,0^-,0)$ level for the emitter of the 28 753 cm^{-1} band. The photoexcitation to the T-shaped AlNC from the several vibrational levels of the linear AlNC and AlCN is found to be negligible.

In the $\tilde{A}$-$\tilde{X}$ emission, the A_{nm} summed up with m of the $\tilde{X}$ state corresponds to the fluorescence decay rate of the n level of the $\tilde{A}$ state, which represents the inverse of the fluorescence lifetime. Figure 10 shows the transition probabilities of 18 bands for the 1 $^1A''$-$\tilde{X}$ emission and the fluorescence lifetimes for the vibrational levels of the 1 $^1A''$ state for AlNC. The $|M|^2$ slightly depends on the vibrational energy for the 1 $^1A''$ state. Nevertheless, we found that the dependence is not so serious and then estimated the transition probabilities averaged over the vibrational levels in the calculated energy range. The similar results are obtained from 12 bands of the 2 $^1A'$-$\tilde{X}$ emission. The $|M|^2$ value averaged 18 bands is $(1.51\pm0.07)e^2a_0^2$ for the 1 $^1A''$-$\tilde{X}$ system and is $(1.37\pm0.07)e^2a_0^2$ for the 2 $^1A'$-$\tilde{X}$ system. The fluorescence lifetimes for the 1 $^1A''$ and 2 $^1A'$ states are evaluated to be 7.2 ± 0.5 ns. For AlCN, the $|M|^2$ value is obtained only for the lowest four levels of the excited state since the FCFs for much higher levels summed up with the vibrational levels of the $\tilde{X}$ state did not reach unity. The $|M|^2$ value is $1.25e^2a_0^2$ for the 1 $^1A''$-$\tilde{X}$ system and is $1.07e^2a_0^2$ for the 2 $^1A'$-$\tilde{X}$ system. The fluorescence lifetimes for the 1 $^1A''$ and 2 $^1A'$ states are evaluated to be 21 and 24 ns, respectively.

IV. SUMMARY

The PESs of the $\tilde{X}$ $^1\Sigma^+$ and $\tilde{A}$ $^1\Pi$ (1 $^1A''$,2 $^1A'$) states of AlNC/CN were obtained with the CASSCF/MRCI method with the aug-cc-pVTZ basis sets in this study. The electronic energies of these states agreed very well with the observed data. The SO effects on the electronic energies of these states

were found to be negligible in the energy region interested in this study. The vibrational energies were calculated and assigned up to 350 levels for each electronic state except the strongly mixed wave functions. Einstein's B coefficients were calculated as the square of the transition moments that depend on both the initial and final vibrational states. The absorption spectra for the linear AlNC and AlCN calculated from Einstein's B coefficients and the fluorescence spectra calculated from Einstein's A coefficients were compared with the observed spectra. The theoretical emission spectra for the $1\,^1A''$-$\tilde{X}$ system agree well with the observed spectra. The emitters for several bands observed for the AlNC($2\,^1A'$-$\tilde{X}$) system were reassigned and the emitters for the two bands observed for AlCN were identified tentatively based on both the profiles of the fluorescence spectra and their transition energies. This study shows that the theoretical method developed for probing electronic transitions has an adequate accuracy to analyze quantitatively available experimental data.

ACKNOWLEDGMENT

The computation was mainly carried out using the computer facilities at the Research Center for Computational Science of The Okazaki National Institutes.

[1] T. Törring, J. P. Bekooy, W. L. Meerts, J. Hoeft, E. Tiemann, and A. Dymanus, J. Chem. Phys. **73**, 4875 (1980).
[2] J. Van Vaals, W. L. Meerts, and A. Dymanus, Chem. Phys. **82**, 385 (1983).
[3] J. Van Vaals, W. L. Meerts, and A. Dymanus, Chem. Phys. **86**, 147 (1984).
[4] A. Dorigo, P. R. von Schleyer, and P. Hobza, J. Comput. Chem. **15**, 322 (1994).
[5] C. W. Bauschlicher, Jr., S. R. Langhoff, and H. Partridge, Chem. Phys. Lett. **115**, 124 (1985).
[6] R. R. Wright and T. A. Miller, J. Mol. Spectrosc. **194**, 219 (1999).
[7] T. Hirano, K. Ishii, T. E. Odaka, and P. Jensen, J. Mol. Spectrosc. **215**, 42 (2002).
[8] M. Fukushima and T. Ishiwata, J. Mol. Spectrosc. **216**, 159 (2002).
[9] T. E. Odaka, T. Hirano, and P. Jensen, J. Mol. Spectrosc. **216**, 379 (2002).
[10] T. Taketsugu, K. Ishii, and S. Carter, Chem. Phys. Lett. **380**, 213 (2003).
[11] M. Douay and P. F. Bernath, Chem. Phys. Lett. **174**, 230 (1990).
[12] C. T. Scurlock, D. A. Fletcher, and T. C. Steimle, J. Chem. Phys. **101**, 7255 (1994).
[13] S. Nanbu, S. Minamino, and M. Aoyagi, J. Chem. Phys. **106**, 8073 (1997).
[14] K. Ishii, T. Taketsugu, and T. Hirano, Chem. Phys. Lett. **374**, 506 (2003).
[15] O. Bludský, V. Špirko, T. E. Odaka, P. Jensen, and T. Hirano, J. Mol. Struct. **695**, 219 (2004).
[16] B. Ma, T. Yamaguchi, and H. F. Schaefer III, Mol. Phys. **86**, 1331 (1995).
[17] J. S. Robinson, A. J. Apponi, and L. M. Ziurys, Chem. Phys. Lett. **278**, 1 (1997).
[18] K. A. Walker and M. C. L. Gerry, Chem. Phys. Lett. **301**, 2000 (1999).
[19] M. Fukushima, Chem. Phys. Lett. **283**, 337 (1998).
[20] I. Gerasimov, X. Yang, and P. J. Dagdigian, J. Chem. Phys. **110**, 220 (1999).
[21] D. K. W. Mok, E. P. F. Lee, F.-T. Chau, and J. M. Dyke, J. Comput. Chem. **16**, 1896 (2001).
[22] D. E. Woon and T. H. Dunning, Jr., J. Chem. Phys. **98**, 1358 (1993), and references therein.
[23] M. R. A. Blomberg and P. E. M. Siegbahn, J. Chem. Phys. **78**, 5682 (1988).
[24] J. Simons, J. Phys. Chem. **93**, 626 (1989).
[25] S. R. Langhoff and D. E. Davidson, Int. J. Quantum Chem. **8**, 61 (1974).
[26] H.-J. Werner and P. J. Knowles, J. Chem. Phys. **89**, 5803 (1988).
[27] P. J. Knowles and H.-J. Werner, Chem. Phys. Lett. **145**, 514 (1988).
[28] H.-J. Werner, P. J. Knowles, R. D. Amos *et al.*, MOLPRO is a package of *ab initio* programs.
[29] D. Shepard, *Proceedings of the 1968 23rd ACM National Conference* (AMC, New York, 1968), p. 517; P. Lancaster and K. Salkauskas, *Curve and Surface Fitting, An Introduction* (Academic, London, 1986), Chap. 10.
[30] K. C. Thompson, M. J. T. Jordan, and M. A. Collions, J. Chem. Phys. **108**, 8302 (1998), and references therein.
[31] T. Ishida and G. C. Schatz, Chem. Phys. Lett. **314**, 369 (1999).
[32] J. V. Lill, G. A. Parker, and J. C. Light, Chem. Phys. Lett. **89**, 483 (1982).
[33] D. T. Colbert and W. H. Miller, J. Chem. Phys. **96**, 1982 (1992).
[34] E. M. Goldfield and S. K. Gray, Comput. Phys. Commun. **98**, 1 (1998).
[35] C.-Y. Yang and S. K. Gray, J. Chem. Phys. **107**, 7773 (1997).
[36] K. M. Forsythe and S. K. Gray, J. Chem. Phys. **112**, 2623 (2000).
[37] R. B. Lehoucq, K. Maschhoff, D. C. Sorensen, and C. Yang, ARPACK (Rice University, Houston, 1997); see the ARPACK homepage, http://www.caam.rice.edu/software/ARPACK/
[38] H. Eyring, J. Walter, and G. E. Kimball, *Quantum Chemistry* (Wiley, New York, 1944), p. 115.
[39] F.-T. Chau, E. P.-F. Lee, D. K.-W. Mok, D.-C. Wang, and J. M. Dyke, J. Electron Spectrosc. Relat. Phenom. **108**, 75 (2000).
[40] G. Igel-Mann, H. Stoll, and H. Preuss, Mol. Phys. **65**, 1321 (1988).
[41] T. H. Dunning, Jr., J. Chem. Phys. **90**, 1007 (1989).
[42] G. Herzberg, *Infrared and Raman Spectra of Polyatomic Molecules*, Molecular Spectra and Molecular Structure Vol. 2 (Van Nostrand, Princeton, NJ, 1945).
[43] G. Herzberg, *Electronic Spectra and Electronic Structure of Polyatomic Molecules*, Molecular Spectra and Molecular Structure Vol. 3 (Van Nostrand, Princeton, NJ, 1966).
[44] N. Richardson, Y. Yamaguchi, and H. F. Schaefer III, J. Chem. Phys. **119**, 12946 (2003).